

Renouncing electroneutrality is not free of charge: Switching on electrogenicity in a Na^+ -coupled phosphate cotransporter

Andrea Bacconi, Leila V. Virkki, Jürg Biber, Heini Murer, and Ian C. Forster*

Institute of Physiology and Center for Integrative Human Physiology, University of Zürich, Winterthurerstrasse 190, CH-8057 Zürich, Switzerland

Communicated by Gerhard Giebisch, Yale University School of Medicine, New Haven, CT, July 14, 2005 (received for review April 28, 2005)

Renal type IIa Na^+ -coupled inorganic phosphate (P_i) cotransporters (NaPi-IIa) mediate divalent P_i transport in an electrogenic manner, whereas the renal type IIc isoform (NaPi-IIc) is electroneutral, yet it shows high sequence identity with NaPi-IIa. Dual uptake ($^{32}\text{P}_i$ / ^{22}Na) assays confirmed that NaPi-IIc displayed Na^+ -coupled P_i cotransport with a 2:1 ($\text{Na}^+:\text{P}_i$) stoichiometry compared with 3:1 established for NaPi-IIa. This finding suggested that the electrogenicity of NaPi-IIa arises from the interaction of an additional Na^+ ion compared with NaPi-IIc. To identify the molecular elements responsible for the functional difference between isoforms, we used chimera and amino acid replacement approaches. Transport activity of chimeras constructed with NaPi-IIa and NaPi-IIc indicated that residues within the first six transmembrane domains were essential for the electrogenicity of NaPi-IIa. Sequence comparison between electrogenic and electroneutral isoforms revealed differences in the charge and polarity of residues clustered in three areas, one of which included part of the predicted third transmembrane domain. Here, substitution of three residues with their NaPi-IIa equivalents in NaPi-IIc (S189A, S191A, and G195D) resulted in a transporter that displayed a 1:1 charge/ P_i coupling, a 3:1 $\text{Na}^+:\text{P}_i$ stoichiometry, and transient currents that resembled pre-steady-state relaxations. The mutant's weaker voltage dependency and 10-fold lower apparent P_i affinity compared with NaPi-IIa indicated that other residues important for the NaPi-IIa kinetic fingerprint exist. Our findings demonstrate that, through a minimal number of side chain substitutions, we can effect a switch from electroneutral to electrogenic cotransporter function, concomitant with the appearance of a cosubstrate interaction site.

Secondary-active transporter proteins mediate uphill transport of a solute by tapping into the free energy provided by the concentration gradient of a coupled ion that is specific to the transporter protein (e.g., H^+ , K^+ , or Na^+). The coupling between driving and driven species confers a strict stoichiometric ratio on cotransport function. When stoichiometrically coupled movement of net charge accompanies cotransport, an additional driving force is available, derived from the free energy established by the transmembrane electric field. For such electrogenic cotransporters, it follows that membrane voltage also becomes a kinetic determinant of the transport mechanism; moreover, under physiological conditions, it can serve to enhance the concentrating ability of the transport protein.

One of the many physiologically important transport processes that rely on a secondary active mechanism is reabsorption of inorganic phosphate (P_i) in the renal proximal tubule. Two isoforms of type II Na^+ -coupled P_i cotransporters (NaPi-II), both localized at the proximal tubule apical brush border membrane, have been identified. Both cotransporters mediate inward transport of P_i by using the inwardly directed Na^+ gradient (1, 2). Type IIa cotransporters (SLC34A1 or NaPi-IIa) couple three Na^+ ions to the cotransport of one divalent P_i ion, and each transport cycle is accompanied by the inward translocation of one net positive charge (3, 4). The NaPi-IIa cotransport rate is strongly dependent on transmembrane potential. This dependency is hypothesized to result from voltage-dependent transitions between favored confor-

mational states of the protein that include the interaction of one Na^+ ion with intrinsic mobile charges of the NaPi-IIa protein (4–9).

In contrast, renal type IIc cotransporters (SLC34A3 or NaPi-IIc) (2, 10) mediate electroneutral Na^+ -coupled P_i cotransport yet, with respect to other steady-state transport parameters (e.g., apparent substrate affinities and pH dependency), resemble NaPi-IIa. Consistent with electroneutral cotransport of divalent P_i , it has been proposed that NaPi-IIc cotransports with a 2:1 $\text{Na}^+/\text{HPO}_4^{2-}$ stoichiometry (2, 10). It follows that NaPi-IIc may lack one of the three Na^+ binding sites postulated for NaPi-IIa. So far, neither the absence of a Na^+ binding site nor the stoichiometry have been experimentally established. Topological prediction algorithms indicate no significant differences between NaPi-IIa and NaPi-IIc (4), which suggests that their respective transmembrane topologies are most likely identical. Moreover, a sequence comparison of NaPi-IIa and NaPi-IIc indicates a high degree of similarity (10), particularly in the predicted transmembrane domain (TMD) regions. These findings imply that only small changes in the amino acid sequence may be required to perform a functional switch between the electrogenic and electroneutral behavior, together with a concomitant change in the stoichiometry.

To identify the molecular elements responsible and gain insight into the underlying mechanism that confers electrogenicity to NaPi-IIa, we took advantage of the functional difference between the NaPi-IIa and NaPi-IIc isoforms by engineering complementary chimeras between each isoform and expressing these in *Xenopus* oocytes. We then refined the localization procedure by using a bioinformatic approach. This approach led to the identification of three residues in the predicted third TMD (TMD-3) that are conserved in all electrogenic NaPi-II transporters so far identified. By substituting the equivalent NaPi-IIa amino acids at these sites in the NaPi-IIc sequence, functional expression of this transport protein in *Xenopus* oocytes displayed Na^+ -dependent P_i -induced steady-state currents and voltage step-induced transient currents, neither of which were observed in oocytes that expressed the WT NaPi-IIc. Our findings document that TMD-3 mutations transformed the electroneutral NaPi-IIc into an electrogenic cotransporter, and we propose that the electrogenicity results from an increase in the number of Na^+ ion binding sites from two to three.

Materials and Methods

Molecular Biology. Chimeras were based on mouse NaPi-IIa (in pSport) and mouse NaPi-IIc (in pT7T3D-Pac, a kind gift from K.-I. Miyamoto, Tokushima University, Tokushima, Japan). To obtain the NaPi-IIa and NaPi-IIc fragments, we introduced new restriction sites at the junctions. The necessary amino acid substitutions were located in predicted TMD linkers, where substitutions are usually well tolerated (11). Mutagenesis and cRNA preparation were

Abbreviations: P_i , inorganic phosphate; NaPi-II, type II Na^+ -coupled P_i cotransporter; TMD, transmembrane domain; PFA, phosphonoformic acid; NI, noninjected; $I-V$, current-voltage.

*To whom correspondence should be addressed. E-mail: iforster@access.unizh.ch.

© 2005 by The National Academy of Sciences of the USA

performed as described in ref. 9. Oocytes were injected with 50 nl of water or with 50 nl of water containing 10 ng of cRNA.

Reagents and Solutions. The solution compositions were as follows. Control superfusate (ND100): 100 mM NaCl/2 mM KCl/1.8 mM CaCl_2 /1 mM MgCl_2 /10 mM Hepes-Tris, pH 7.4, unless otherwise stated. For pH <6.2, Mes was substituted for Hepes. Na^+ -free superfusate (ND0): as for ND100 with isosmotic substitution of choline Cl for NaCl. Solutions with intermediate Na^+ concentrations were prepared by mixing ND0 and ND100 in appropriate proportions. Substrate test solutions: P_i was added from 1 M K_2HPO_4 and KH_2PO_4 stocks premixed to give the required pH. Phosphonoformic acid (PFA) was added from 100 mM stock.

Functional Assays and Data Analysis. Uptake assays ($^{32}\text{P}_i$ and ^{22}Na) are described in refs. 3 and 9 and typically involved 5–9 oocytes per group. For the dual $^{32}\text{P}_i$ / ^{22}Na uptake, the Na^+ concentration was lowered to 40 mM to achieve a high enough specific activity for ^{22}Na with 2 mM total P_i . Electrophysiology was performed with a two-electrode voltage clamp (5). Simultaneous uptake and electrophysiology were performed on single oocytes with a chamber designed by D. D. F. Loo (University of California, Los Angeles), which was perfused at 50 $\mu\text{l}/\text{min}$ with a peristaltic pump (3). Steady-state current–voltage (I – V) relations were determined by using a voltage staircase from -120 mV to $+40$ mV with 100-ms steps (5) and by subtracting the control response in the absence of substrate from the test response.

The P_i and Na^+ activation kinetics were determined as described in ref. 8. Proton dependency was determined in ND100 with pH ranging from 5.0 to 8.0 and total P_i adjusted to give 1 mM divalent P_i . Transient currents were acquired by using voltage steps from a holding potential (V_h) = -60 mV to test potentials in the range -160 mV to $+80$ mV as described (9). Charge (Q) was quantified by fitting a single exponential commencing ≈ 6 ms after the step onset, extrapolating this to the step onset, and performing numerical integration.

Data points are shown as mean \pm SEM. Curve fitting to data points was performed by using nonlinear regression analysis (PRISM, GraphPad, San Diego).

Results and Discussion

Dual Uptake Assays Establish That NaPi-IIa and NaPi-IIc Have Different Stoichiometries. In two previous studies, the cotransport stoichiometry of rat NaPi-IIa, flounder NaPi-IIb (3), and human NaPi-IIa (9) isoforms were determined under voltage clamp conditions and yielded a Na/P_i /charge ratio of 3:1:1. This ratio is consistent with the inward translocation of one net charge per transport cycle, given that divalent P_i is the preferred species transported. To determine the stoichiometry of the electroneutral NaPi-IIc, we performed a dual uptake ($^{32}\text{P}_i$ and ^{22}Na) assay at pH 7.4 and plotted ^{22}Na uptake against $^{32}\text{P}_i$ uptake for each oocyte (Fig. 1). The fitted slope of a linear regression line was 2.0 ± 0.2 for $n = 19$ oocytes from three donor frogs, which was consistent with electroneutral cotransport of two Na^+ ions for each HPO_4^{2-} ion.

To investigate whether membrane potential influenced the rate of $^{32}\text{P}_i$ uptake by NaPi-IIc, we performed a $^{32}\text{P}_i$ assay on individual oocytes that were voltage-clamped at -20 or -80 mV. NaPi-IIc expressing oocytes clamped to -20 mV gave an uptake rate (expressed as pmol per oocyte per minute) of 42 ± 8 ($n = 9$) compared with 44 ± 8 ($n = 9$) at -80 mV. Control oocytes from the same donor frog gave uptakes of 6 ± 3 ($n = 4$) and 3 ± 1 ($n = 4$) at -20 mV and -80 mV, respectively. These data confirmed that in this voltage range, the NaPi-IIc cotransport cycle did not include rate-determining voltage-dependent transitions (12).

Chimeras Localize NaPi-IIa Electrogenicity to Sites in the First Six TMDs. To identify the molecular elements that distinguish the electrogenic and stoichiometric properties of NaPi-IIa from those

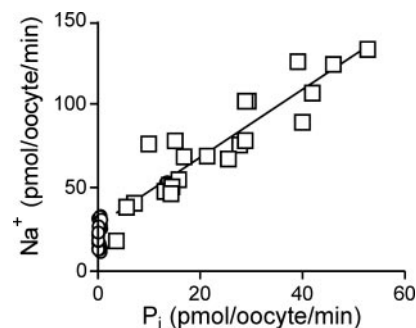


Fig. 1. NaPi-IIc has a 2:1 cotransport stoichiometry. Dual $^{22}\text{Na}/^{32}\text{P}_i$ uptake assay data for oocytes expressing NaPi-IIc (\square) and control oocytes (\circ) from the same donor frog. Slope of linear regression line: 2.0 ± 0.2 .

of NaPi-IIc, our first strategy was to engineer chimeras between each cotransporter. The chimeras were based on a consensus topological model for NaPi-II proteins comprising eight TMDs and intracellular N and C termini predicted by a hydrophobicity analysis (4) (Fig. 2A). We split the primary sequences at convenient sites in the predicted linker regions to preserve the structural integrity of the TMDs to make six chimeric constructs that comprised complementary sections of the C-terminal and N-terminal parts of each full-length protein (Fig. 2B). We also constructed two triple chimeras in which a central portion of NaPi-IIa or NaPi-IIc that comprised five TMDs was inserted between the complementary N terminus plus the first TMD and the C terminus plus the last two TMDs, respectively. For all chimeras, we left intact the native amino acid sequence that included the first intracellular and third extracellular linkers (ICL-1 and ECL-3, respectively) and the two

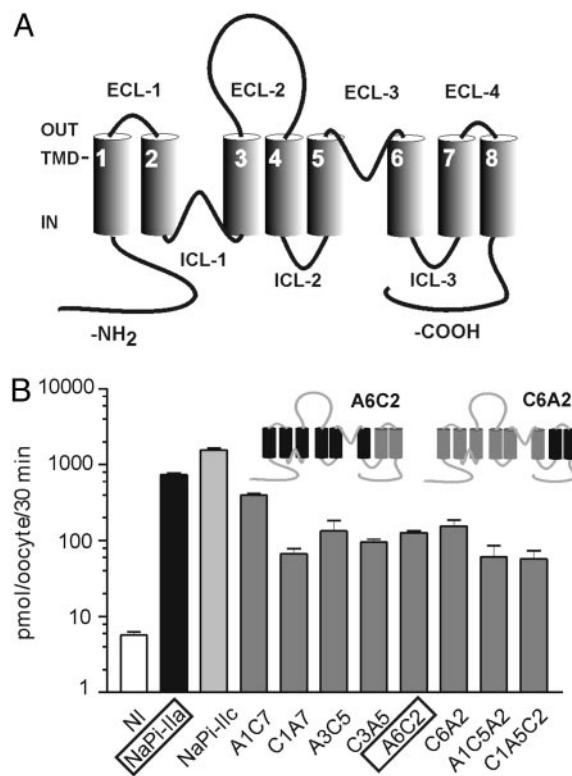


Fig. 2. Chimeras of NaPi-IIc and NaPi-IIa localize elements critical for the NaPi-IIa electrogenic phenotype to TMDs 1–6. (A) Topology of NaPi-II protein based on hydrophobicity analysis. (B) $^{32}\text{P}_i$ uptake of chimeras compared with WT NaPi-IIc and NaPi-IIa. (Inset) Example of chimera composition for A6C2 and C6A2.

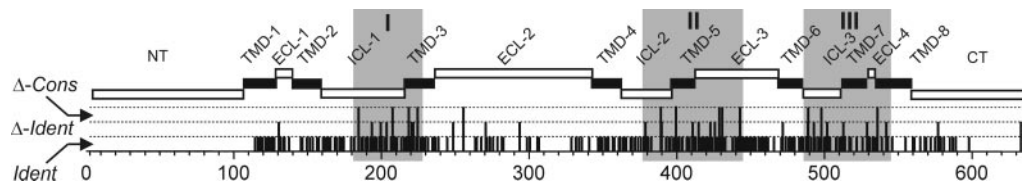


Fig. 3. Sequence comparison of NaPi-IIa/c. Multiple sequence alignment indicates position of residues that are 100% identical in all 21 candidate sequences (*Ident*), changed between putative electrogenic and electroneutral sequences with 100% identity at the respective site (Δ -*Ident*) or changed with conservative substitutions in either or both groups (Δ -*Cons*). Shaded areas (I, II, and III) indicate clusters of changed residues. Residue numbering is according to mouse NaPi-IIa sequence. Topological designation shows position and relative lengths of TMDs and linker stretches as predicted by hydrophobicity analysis. NT, N-terminal; CT, C-terminal.

neighboring TMDs. These linkers are present in all NaPi-II isoforms and are thought to contain structural motifs that define the cotransport pathway (13–15).

The $^{32}\text{P}_i$ uptake from oocytes expressing each chimera was noticeably smaller than the uptake obtained from oocytes that expressed either WT transporter (Fig. 2*B*). However, the activity was at least 10-fold higher than noninjected (NI) oocytes from the same donor frog, which indicated that functional chimeras were targeted to the oocyte plasma membrane. Despite this low activity, we expected that P_i -induced electrogenic responses would be detectable over and above any endogenous oocyte activity (3).

Whether chimeras were electrically active or silent allowed us to draw conclusions about the localization of determinants of electrogenicity. First, replacement of the last two TMDs of NaPi-IIa with the corresponding stretch from NaPi-IIc (chimera A6C2) gave a construct that was still electrogenic. Application of 1 mM P_i induced an inward current under voltage clamp [-42 ± 4 nA ($n = 5$) at -60 mV] that was clearly larger than the magnitude of the endogenous response, observed for NI oocytes (typically <5 nA under the same conditions) (data not shown). A6C2 showed a weaker steady-state voltage dependency than the NaPi-IIa WT. For NaPi-IIa, a change in membrane voltage from 0 to -100 mV resulted in an $\approx 60\%$ increase in P_i -induced current (for an example, see Fig. 4*D*), whereas A6C2 showed only an $\approx 20\%$ increase (data not shown). Moreover, at -50 mV the estimated apparent affinity for P_i ($K_m^{\text{P}_i}$) was 0.82 ± 0.08 mM, which was significantly larger than for WT NaPi-IIa determined from cells from the same donor frog (0.14 ± 0.01 mM). Although the small magnitude of the P_i -induced currents for A6C2 precluded further detailed kinetic characterization, these findings indicated that kinetic determinants of the NaPi-IIa fingerprint, including voltage dependency, were also located within the stretch that included the last two TMDs of NaPi-IIa. As expected, the reciprocal chimera (C6A2) was electrically silent but exhibited $^{32}\text{P}_i$ uptake comparable with A6C2. Second, starting from A6C2, we replaced its TMD-1 with that from NaPi-IIc in an attempt to narrow down the critical region. This triple chimera (C1A5C2) showed $^{32}\text{P}_i$ uptake comparable with A6C2, but it was electrically silent, which suggested that TMD-1 was also critical for conferring electrogenic behavior to NaPi-IIa. We confirmed this idea by replacement of TMD-1 from NaPi-IIc alone, which gave a functional but electrically silent chimera (C1A7). Moreover, we concluded that TMD-1 from NaPi-IIa was, by itself, insufficient to confer electrogenicity to NaPi-IIc by documenting that the dual (A1C7) and triple (A1C5A2) chimeras were electrically silent. Finally, we retained TMDs 1–3 of NaPi-IIa and replaced TMDs 4–8 of the NaPi-IIa sequence with the corresponding elements from NaPi-IIc. This chimera (A3C5) was functional but electrically silent, which suggested that, in addition to TMD-1, elements critical for the electrogenicity of NaPi-IIa must also reside in the stretch involving TMDs 4–6.

The chimera study indicated that although elements were distributed throughout the protein that contribute to the NaPi-IIa electrogenicity, essential residues were most likely located in the region encompassing TMDs 1–6.

Sequence Alignment Reveals Altered Polarity and Charge of Residues in NaPi-IIc.

Our second strategy involved making a multiple sequence alignment of four currently available mammalian NaPi-IIc sequences and 17 sequences of NaPi-IIa as well as NaPi-IIb isoforms, several of which mediate P_i -dependent electrogenic activity when expressed in oocytes (3, 16–19). The alignment showed that, among the 21 sequences (excluding the N and C termini and ECL-2, where large variations are observed between isoforms), $\approx 75\%$ of residues were 100% identical or in a few cases involved conservative substitutions (Fig. 3, *Ident*). The alignment revealed 22 sites that differed between each group but were 100% identical within the respective group (Fig. 3, Δ -*Ident*). In addition, we identified a further 13 sites that differed between electrogenic and electroneutral transporters and involved conservative substitutions among members of each group (Fig. 3, Δ -*Cons*). Interestingly, the majority of changed sites clustered into three areas (Fig. 3, shaded boxes): cluster I comprised nine residues distributed in the second half of ICL-1 and the first half of TMD-3; cluster II comprised 10 residues in TMD-5 and its neighboring linkers, ICL-2 and ECL-3; and cluster III comprised eight residues distributed within the

Table 1. Changes in residues belonging to clusters from multiple sequence alignment

Cluster	Site	Polarity	Charge
I	A184S/C	+/-	
	I193V	+	
	N199S	-	
	A203S	+	
	A/V207S	+	
	A218S/G	+	
	A220S	+	
	T221A	-	
	D224G/S		-(-)
II	Q378R		+(+)
	T/Q389A	-	
	T/A489G/S	+	
	M410L	+	
	V414L	-	
	S422A	-	
	T425V	-	
	I/V428M	-	
	I/L430V	+	
III	T/S442L/F	-	
	P488L/V	-	
	T492L	-	
	R/H497P		-(+)
	L502F	-	
	F512V	+	
V528A	+		
W536G/S	+		
G541A	-		

Each entry refers to a residue in consensus electrogenic transporters that has been changed in the NaPi-IIc sequence. Numbering refers to mouse NaPi-IIa sequence. +/- indicates increase/decrease in polarity or charge, respectively, according to a hydrophobicity scale (25).

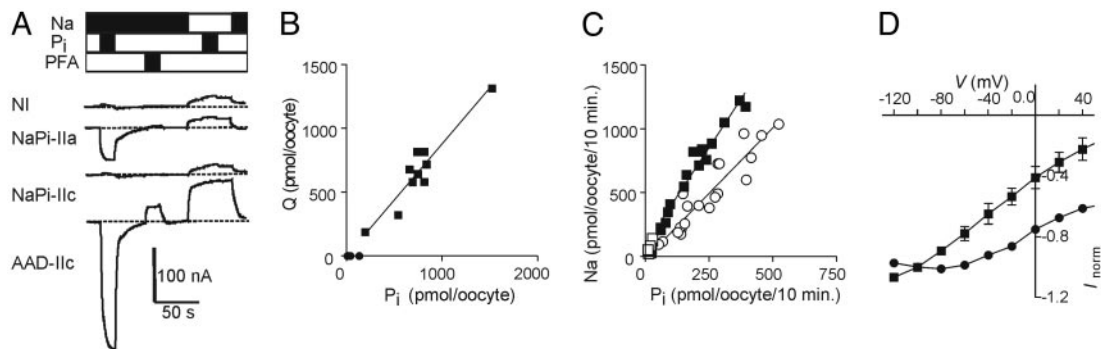


Fig. 4. Steady-state properties of the triple mutant AAD-IIC. (A) Representative current tracings of oocytes from the same batch, comparing NI, NaPi-IIa, NaPi-IIC, and AAD-IIC under the superfusion conditions indicated. Na, ND100; Pi, ND100 plus 1 mM Pi; PFA, ND100 plus 1 mM PFA. Oocytes were voltage-clamped at -50 mV. (B) Net charge translocated plotted as a function of Pi uptake for individual oocytes expressing AAD-IIC (■) and control oocytes from the same donor frog (●). Slope of linear regression line: 0.9 ± 0.1 . (C) Dual uptake for AAD-IIC (■) and control oocytes (□) from the same donor frog. Slope of linear regression line: 3.0 ± 0.2 . For comparison purposes, the data of Fig. 1 for the WT NaPi-IIC have been replotted with the respective mean of control oocytes subtracted (○). (D) Normalized I-V plots that compare NaPi-IIa (■, $n = 5$) and AAD-IIC (●, $n = 6$). Each data point is the difference between the currents recorded in ND100 plus 1 mM Pi and ND100, respectively, at a given V . Data for each cell were normalized to the Pi-induced current at -100 mV.

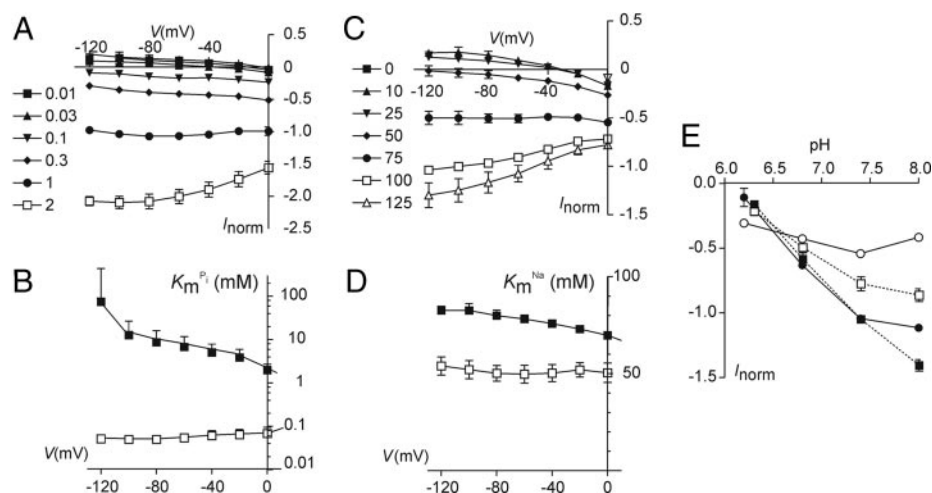
region, including ICL3 and the last two TMDs. The distribution of changed residues between electrogenic and electroneutral transporters was consistent with the findings of the chimera study. Surprisingly, TMD-1 contained no nonconserved substitutions; yet, from the chimera study, we concluded that its presence was essential for conferring electrogenic behavior to NaPi-IIa. This requirement might be a consequence of our choice of restriction site for constructing the C1A7 chimera, whereby the part of ECL-1 that contains a Gly-Ser substitution in all NaPi-IIC isoforms was included with TMD-1. In contrast, Cys substitution at this site does not alter the electrogenic properties of NaPi-IIa, which indicated that the residue at this site was not a critical determinant of electrogenic behavior but may play a modulatory role (8).

Next, we focused on the amino acid changes in the three clusters (Table 1). We categorized the changes in terms of polarity and charge, because these properties would potentially affect the electrogenic behavior and substrate coordination. Cluster I showed the most significant changes with the majority of substitutions involving an increase in side-chain polarity (most commonly Ala→Ser) and removal of negative charge at site 224 (Asp→Gly/Ser). Significantly, this charge is conserved in all putative electrogenic trans-

porters, particularly in view of the finding that substituting Asp-224 in human NaPi-IIa with Gly resulted in electroneutral Pi transport (L.V.V., I.C.F., A.B., J.B., and H.M., unpublished data). In contrast, clusters II and III showed mixed changes in polarity, together with a gain and loss of positive charge at sites 380 and 499, respectively. Furthermore, cluster III included TMDs 7 and 8 and ECL-4, which we showed were not essential for preserving electrogenic behavior in NaPi-IIa (Fig. 2B) but could nevertheless play a modulatory role, as evidenced by the weak voltage dependency of chimera A6C2 and Cys mutagenesis studies in ECL-4 (7, 8).

Substitution of NaPi-IIa Residues in TMD-3 Confers Electrogenicity to the NaPi-IIC Backbone. Next we investigated the impact of the residue changes in TMD-3 by using NaPi-IIC as a backbone into which we substituted the equivalent NaPi-IIa residues. When we substituted Gly-195 with the NaPi-IIa equivalent Asp-224 (mutant D-IIC) or Ser-189 and Ser-191 with the NaPi-IIa equivalents Ala-218, Ala-224 (mutant AA-IIC), we obtained functionally expressed mutants as evidenced by Na⁺-dependent ³²Pi uptakes that were significantly greater than NI cells (data not shown). However, in neither case

Fig. 5. Substrate dependency of AAD-IIC. (A) I-V plots for Pi activation. Data for individual oocytes were determined for the Pi concentrations indicated (in mM) and data for each cell were normalized to the Pi-dependent current at 1 mM Pi and -100 mV ($n = 4$). (B) Apparent affinity for Pi-activation (K_m^{Pi}) for NaPi-IIa (□, $n = 3$) and AAD-IIC (■, $n = 4$) as found by fitting a form of the Michaelis-Menten equation, $I_{Pi} = I_{Pi}^{max} ([Pi]/([Pi] + K_m^{Pi}) + K)$, to the data of A at each membrane potential, where $[Pi]$ is the Pi concentration, K_m^{Pi} is the apparent affinity for Pi, I_{Pi}^{max} is the maximum cotransport rate, and K is a variable offset (7). Note the logarithmic ordinate scale. (C) I-V plots for Na⁺ activation. Data for individual oocytes were determined for the Na⁺ concentrations indicated (in mM) with 1 mM Pi, and data for each cell were normalized to the Pi-dependent current at 1 mM Pi and -100 mV ($n = 4$). (D) Apparent affinities for Na⁺ activation (K_m^{Na}) for NaPi-IIa (□, $n = 4$) and AAD-IIC (■, $n = 4$) as reported from fitting a form of the modified Hill equation: $I_{Pi} = I_{Pi}^{max} \{ [Na]^{n_H} / ([Na]^{n_H} + (K_m^{Na})^{n_H}) \} + K$, to the data of panel C at each membrane potential, where $[Na]$ is the concentration of Na⁺, n_H is the Hill coefficient, K_m^{Na} is the apparent affinity for Na⁺. (E) Proton dependency for NaPi-IIa (circles, continuous lines) and AAD-IIC (squares, dotted lines) at 0 mV (open symbols) and -120 mV (filled symbols). Data for NaPi-IIa ($n = 5$) and AAD-IIC ($n = 5$) were normalized to the response to 1 mM HPO₄²⁻ at -100 mV, pH 7.4. Current reversal at low substrate concentrations in A and C results from the subtraction of the uncoupled leak current (7, 9).



could we detect P_i -induced currents. For mutant D-IIC, where the $^{32}P_i$ uptake was only ≈ 4 -fold greater than the NI uptake, we were nevertheless confident that electrogenic activity should have been detectable, because this uptake rate would correspond to currents with a magnitude >10 nA. Remarkably, after we substituted all three NaPi-IIa residues at the corresponding sites in NaPi-IIC, the triple NaPi-IIC mutant (AAD-IIC) displayed Na^+ -dependent $^{32}P_i$ uptake and a P_i -induced electrogenic response (Fig. 4). When challenged with 1 mM P_i in ND100, AAD-IIC gave robust, inward currents (typically in the range 50–250 nA) at -50 mV; in zero external Na^+ (ND0), no significant current was detected under the same conditions (Fig. 4A). Furthermore, we did not detect a response to P_i when Li^+ was substituted for Na^+ (data not shown), which indicated that AAD-IIC had retained the NaPi-II specificity for Na^+ as its cosubstrate. Like WT NaPi-IIa, AAD-IIC also responded to the Na^+ P_i cotransporter inhibitor, PFA, which was evidence of block for a Na^+ -dependent leak current associated with the expressed cotransporter protein (5). Neither control (NI) nor NaPi-IIC-expressing oocytes from the same donor frog showed significant responses to P_i or PFA under the same superfusion conditions (Fig. 4A). The holding current decrease observed after removal of external Na^+ was in part due to endogenous Na^+ -dependent channels and a transporter-related leak.

To determine whether the P_i -induced currents were stoichiometrically coupled to P_i cotransport, we assayed the charge and $^{32}P_i$ uptake on individual voltage-clamped oocytes ($V_h = -50$ mV). This assay yielded a slope of 0.9 ± 0.1 , which established that AAD-IIC transported one net charge per cotransported P_i molecule (Fig. 4B). Moreover, by dual $^{22}Na/^{32}P_i$ uptake, we documented a slope of 3.0 ± 0.2 , which indicated a 3:1 Na/ P_i stoichiometry (Fig. 4C). Taken together, these findings demonstrate conclusively that the three TMD-3 mutations alone were sufficient to establish Na^+ -coupled electrogenic P_i cotransport in the electroneutral NaPi-IIC backbone, namely a Na/ P_i /charge stoichiometry of 3:1:1. Moreover, the increased Na/ P_i stoichiometry suggests that the mutagenesis had revealed a new Na^+ interaction site.

The steady-state voltage dependency of AAD-IIC was, however, clearly weaker than NaPi-IIa when the normalized I–V data were compared (Fig. 4D). This finding indicated that residue changes at other sites in the NaPi-IIC backbone would be necessary to establish the type IIa electrogenic profile.

AAD-IIC Shows Altered Substrate Activation Characteristics. The P_i cotransport kinetics for NaPi-IIC (10) are similar to those previously reported for NaPi-IIa isoforms from several mammalian species (5, 9, 20), i.e., similar apparent affinities for P_i and Na^+ and a strong proton dependency. This finding suggested that both isoforms share the same molecular elements for substrate recognition and interaction and, importantly, that these processes are not directly dependent on the electrogenic properties of the transporter. To investigate whether engineering in TMD-3 had altered these parameters, we assayed the P_i , Na^+ , and H^+ dependency of AAD-IIC under voltage clamp.

P_i -dependent currents in 100 mM Na^+ (pH 7.4) showed a weak voltage dependency even up to 2 mM total P_i , with no evidence of saturation for potentials in the range -120 mV $\leq V \leq 0$ mV (Fig. 5A). At higher substrate concentrations, P_i complexed with divalent cations in ND100 solution, thereby rendering the estimate of free P_i uncertain. Because oocytes were electrically unstable in divalent-free conditions, we were unable to achieve saturating activation, which resulted in a large uncertainty in the estimate of $K_m^{P_i}$ (Fig. 5B). Nevertheless, this parameter was ≈ 10 -fold larger than the values documented in this study for NaPi-IIa or for NaPi-IIC determined from $^{32}P_i$ uptake (10) (70 μ M). Whereas $K_m^{P_i}$ for NaPi-IIa showed a weak increase with depolarization, as previously reported for the rat isoform (5), the estimates of $K_m^{P_i}$ for AAD-IIC reported by the fit suggested an inverse relationship with membrane potential. However, the fit uncertainties precluded drawing a definite conclusion.

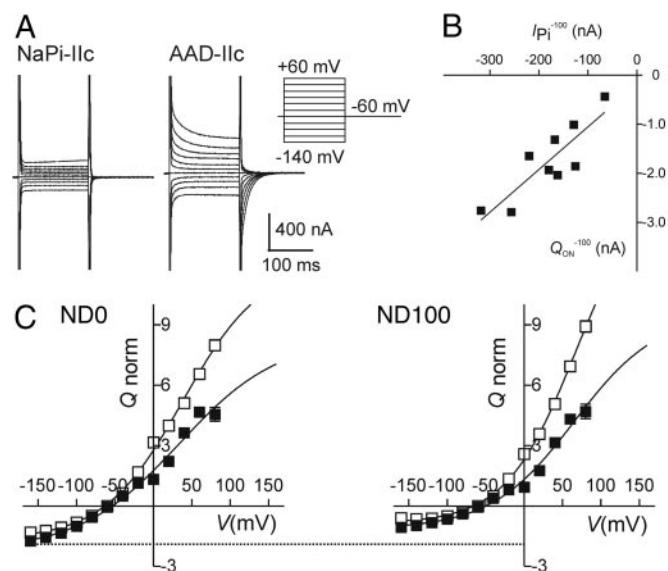


Fig. 6. Voltage steps induce transient currents. (A) Currents recorded in response to a series of voltage steps in the range -140 mV to $+60$ mV from a -60 mV holding potential for a representative WT NaPi-IIC- and AAD-IIC-expressing oocyte from the same donor frog (superfusion in ND100). (B) Correlation of charge movement for AAD-IIC induced by a voltage step from -60 mV to -100 mV for superfusion in ND0, with the steady-state current induced by 1 mM P_i at -100 mV (superfusion in ND100). Line is a linear regression, with $r^2 = 0.74$, $n = 9$. (C) Normalized charge–voltage (Q – V) data for superfusion in ND0 and ND100 for the same batch of AAD-IIC-expressing oocytes ($n = 8$). The charge induced by a voltage step from -60 mV to -100 mV (in ND0) was used to normalize data for each cell before pooling. Error bars smaller than symbols are not shown. \square indicates ON charge movement from -60 mV to target potential. \blacksquare indicates OFF charge movement from target potential to -60 mV. Continuous lines are fits to data using a Boltzmann equation of the form: $Q = Q_{hyp} + Q_{max}/[1 + \exp(-ze(V - V_{0.5})/kT)]$, where Q_{max} is the maximum charge translocated, Q_{hyp} is the steady-state charge at the hyperpolarizing limit and depends on V_h , $V_{0.5}$ is the voltage at which the charge is distributed equally between two hypothetical states, z is the apparent valency per cotransporter, e is the elementary charge, k is Boltzmann's constant, and T is the absolute temperature. The dashed line indicates the hyperpolarizing limit for ON charge movement with ND0 superfusion.

In contrast to P_i activation, Na^+ activation at constant P_i (1 mM) showed a saturating electrogenic response (Fig. 5C). The activation characteristic for a given $V < 0$ mV was sigmoidal with an inflection at low Na^+ (data not shown), indicative of a system in which more than one Na^+ ion interacted with the protein per transport cycle. Compared with NaPi-IIa, the apparent affinity for Na^+ (K_m^{Na}) of AAD-IIC was $\approx 50\%$ greater and slightly increased with depolarization (Fig. 5D).

Finally, we examined the effect of external acidification on AAD-IIC because protons are known to modulate the kinetics of electrogenic type II Na^+/P_i cotransporters (5, 6, 9, 16). To eliminate errors from the titration of P_i , we maintained the divalent P_i at 1 mM so that any change in activity would reflect the effect of protons on the cotransport rate. At $V = 0$ mV, a pH change from 7.4 to 6.2 gave a 43% loss of electrogenic activity for NaPi-IIa compared with 80% for AAD-IIC under the same conditions (Fig. 5E). The latter result is consistent with the reported NaPi-IIC pH dependency data (10, 21) when account is taken of the reduced availability of divalent P_i and suggested that AAD-IIC has preserved the proton sensitivity of NaPi-IIc. In contrast, at $V = -120$ mV, both AAD-IIC and NaPi-IIa showed similar dependency for $5.0 \leq pH \leq 7.4$. These findings suggest that mutagenesis in the NaPi-IIC backbone has established the same proton interaction mechanism in AAD-IIC as for NaPi-IIa (6, 9).

AAD-IIC Displays Transient Currents Related to Transport Function. A common kinetic feature of electrogenic cotransporters is that voltage steps induce transient currents referred to as pre-steady-state relaxations (5, 22). We documented robust transient currents in AAD-IIC-expressing oocytes (Fig. 6A). These currents were easily distinguishable from the oocyte linear capacitive charging and were undetectable in oocytes that expressed NaPi-IIC, which we confirmed to mediate substantial $^{32}\text{P}_i$ uptake, and NI oocytes from the same donor frog (data not shown). We also detected transient currents in the absence of external Na^+ , which suggested that the TMD-3 mutations introduced mobile charges to the NaPi-IIC backbone. We note that our inability to detect transient relaxations in NaPi-IIC does not necessarily exclude the possibility that it has charges that respond to the transmembrane field, but they are immobilized over the range of potentials used.

The magnitude of the charge in ND0 for a 40-mV step to -100 mV correlated with the P_i -induced steady-state currents at -100 mV (Fig. 6B) for oocytes with different steady-state cotransport activities. These data indicate that the transient currents were directly associated with the amount of functionally expressed AAD-IIC in the membrane. We determined the voltage dependency of the charge movements in the range -160 mV to $+80$ mV for superfusion in ND0 and ND100 (Fig. 6C). Because pre-steady-state relaxations reflect the reversible movement of a fixed number of charges, we expected charge balance and saturation of charge movement at extreme potentials. These criteria were only satisfied for hyperpolarizing voltage steps, where we documented clear evidence of saturation and $<20\%$ error in charge balance. The rate-limiting behavior of charge movement for steps to hyperpolarizing potentials also agreed with the steady-state I-V data for AAD-IIC (Fig. 4D), which exhibited similar behavior for $V < 0$. This finding strongly suggested that the transient currents were directly associated with the AAD-IIC transport cycle. Moreover, the charge at the hyperpolarizing limit in ND100 was suppressed by $\approx 50\%$ compared with ND0 (Fig. 6C). This finding suggests that the interaction of external Na^+ ions with the protein had immobilized part of the intrinsic charge movement. Importantly, this interaction occurred in the absence of P_i , in support of an ordered kinetic scheme for Na^+ -coupled electrogenic transport in which the binding of one Na^+ ion precedes P_i binding (5).

For depolarizing steps, the corresponding ON charge was significantly smaller than the OFF charge that accompanied a return to -60 mV from depolarizing voltages. It is possible that some charge was missed by the fitting procedure if, for example, a very fast component were masked by the oocyte charging transient. In contrast, the monotonic increase in charge and initial amplitude with starting potential in the OFF transient suggested the involvement of another mechanism. For example, part of the transient current could be resistive and reflect voltage-dependent closure of a channel-like pore, as suggested for the 5HT transporter (23, 24). A fit of the ON charge movements with a Boltzmann function reported midpoint po-

tentials ($V_{0.5}$) of $+22 \pm 12$ mV ($n = 7$) in ND0 and $+61 \pm 14$ mV ($n = 7$) in ND100 and a paired t test indicated that the shift in $V_{0.5}$ was statistically significant ($P = 0.05$). The apparent valencies (z) were 0.42 ± 0.03 ($n = 7$) in ND0 and 0.47 ± 0.04 ($n = 7$) in ND100. These were similar to values reported for NaPi-IIa (5, 8, 9) and NaPi-IIb isoforms (6, 16).

In terms of an alternating access model for cotransport, whereby the empty carrier can assume either an outward or inward facing conformation, depending on the transmembrane electric field, the positive $V_{0.5}$ suggested that for $V \leq 0$, AAD-IIC already favors an outward conformation that would allow Na^+ ions easy access to their binding site. When Na^+ ions interact with AAD-IIC, the intrinsic charge movements are constrained so that stronger depolarization is required to mobilize charge, consistent with the more positive $V_{0.5}$ in ND100. This result is in agreement with the rate-limiting behavior and weak voltage dependency of the steady-state P_i -activation (Fig. 4D). AAD-IIC differs from NaPi-IIa isoforms, which typically show a $V_{0.5}$ in the range -20 to -60 mV (5, 6, 9) and which we previously interpreted as evidence of the empty carrier occupying an inwardly facing conformation at $V = 0$ that changes to outward facing with increasing membrane hyperpolarization (7).

Conclusions

AAD-IIC displays three characteristics unique to Na^+ -dependent electrogenic P_i cotransport: 3:1 Na^+/P_i stoichiometry, 1:1 P_i /charge coupling, and transient charge movements that correlate with steady-state activity. These findings suggest that (i) mutagenesis of the NaPi-IIC backbone has created, directly or indirectly, a Na^+ interaction site, the occupancy of which leads to the stoichiometric translocation of an additional Na^+ ion per transport cycle; (ii) P_i -induced steady-state currents result from a net movement of $+1$ charge per cycle; and (iii) the voltage dependency of the transient charge movements is a direct determinant of the steady-state voltage dependency.

Detailed kinetic analysis of AAD-IIC and comparison with the typical fingerprint of electrogenic type NaPi-IIa/b cotransporter isoforms also revealed significant functional differences: a weak steady-state voltage dependency, which, according to the alternating access model, suggested that the empty carrier favors an outward-facing conformation for $V < 0$, a low apparent affinity for P_i , and a transient charge imbalance that may indicate that the mutagenesis has created a channel-like leakage pathway. These differences underscore the complexity of structure-function relationships and indicate that mutagenesis at other sites is required to establish the typical electrogenic behavior in the NaPi-IIC backbone.

We thank Dr. Anne-Kristine Meinild for helpful discussions. This work was supported by grants from the Swiss National Science Foundation, the Hartmann Müller-Stiftung, the Olga Mayenfisch-Stiftung, the Union Bank of Switzerland, and the Gebert Rüt Stiftung (to H.M.).

- Murer, H., Hernando, N., Forster, I. C. & Biber, J. (2000) *Physiol. Rev.* **80**, 1373–1409.
- Miyamoto, K., Segawa, H., Ito, M. & Kuwahata, M. (2004) *Jpn. J. Physiol.* **54**, 93–102.
- Forster, I. C., Loo, D. D. & Eskandari, S. (1999) *Am. J. Physiol.* **276**, F644–F649.
- Forster, I. C., Kohler, K., Biber, J. & Murer, H. (2002) *Prog. Biophys. Mol. Biol.* **80**, 69–108.
- Forster, I. C., Hernando, N., Biber, J. & Murer, H. (1998) *J. Gen. Physiol.* **112**, 1–18.
- Forster, I. C., Biber, J. & Murer, H. (2000) *Biophys. J.* **79**, 215–230.
- Ehnes, C., Forster, I. C., Bacconi, A., Kohler, K., Biber, J. & Murer, H. (2004) *J. Gen. Physiol.* **124**, 489–503.
- Ehnes, C., Forster, I. C., Kohler, K., Bacconi, A., Stange, G., Biber, J. & Murer, H. (2004) *J. Gen. Physiol.* **124**, 475–488.
- Virkki, L. V., Forster, I. C., Biber, J. & Murer, H. (2005) *Am. J. Physiol.* **288**, F969–F981.
- Segawa, H., Kaneko, I., Takahashi, A., Kuwahata, M., Ito, M., Ohkido, I., Tatsumi, S. & Miyamoto, K. (2002) *J. Biol. Chem.* **277**, 19665–19672.
- de La Horra, C., Hernando, N., Forster, I. C., Biber, J. & Murer, H. (2001) *J. Physiol.* **531**, 383–391.
- Lester, H. A., Mager, S., Quick, M. W. & Corey, J. L. (1994) *Annu. Rev. Pharmacol. Toxicol.* **34**, 219–249.
- Lambert, G., Forster, I. C., Stange, G., Kohler, K., Biber, J. & Murer, H. (2001) *J. Gen. Physiol.* **117**, 533–546.
- Kohler, K., Forster, I. C., Stange, G., Biber, J. & Murer, H. (2002) *Am. J. Physiol.* **282**, F687–F696.
- Kohler, K., Forster, I. C., Stange, G., Biber, J. & Murer, H. (2002) *J. Gen. Physiol.* **120**, 693–705.
- Forster, I. C., Wagner, C. A., Busch, A. E., Lang, F., Biber, J., Hernando, N., Murer, H. & Werner, A. (1997) *J. Mem. Biol.* **160**, 9–25.
- Hilfiker, H., Hattenhauer, O., Traebert, M., Forster, I. C., Murer, H. & Biber, J. (1998) *Proc. Natl. Acad. Sci. USA* **95**, 14564–14569.
- Nalbant, P., Boehmer, C., Dehmelt, L., Wehner, F. & Werner, A. (1999) *J. Physiol.* **520**, 79–89.
- Graham, C., Nalbant, P., Scholermann, B., Hentschel, H., Kinne, R. K. & Werner, A. (2003) *Am. J. Physiol.* **284**, F727–F736.
- Hartmann, C. M., Wagner, C. A., Busch, A. E., Markovich, D., Biber, J., Lang, F. & Murer, H. (1995) *Pflügers Arch.* **430**, 830–836.
- Ohkido, I., Segawa, H., Yanagida, R., Nakamura, M. & Miyamoto, K. (2003) *Pflügers Arch. Eur. J. Physiol.* **446**, 106–115.
- Loo, D. D., Hazama, A., Supplisson, S., Turk, E. & Wright, E. M. (1993) *Proc. Natl. Acad. Sci. USA* **90**, 5767–5771.
- Li, M., Farley, R. A. & Lester, H. A. (2002) *FEBS Lett.* **513**, 247–252.
- Mager, S., Min, C., Henry, D. J., Chavkin, C., Hoffman, B. J., Davidson, N. & Lester, H. A. (1994) *Neuron* **12**, 845–859.
- Engelman, D. M., Steitz, T. A. & Goldman, A. (1986) *Annu. Rev. Biophys. Biophys. Chem.* **15**, 321–353.